

## Influence of initial conditions in low-pressure chamber on the degree of expansion of the boiling liquid nitrogen jet

© R.Kh. Bolotnova<sup>1</sup>, V.A. Korobchinskaya<sup>1,2</sup>, E.F. Gainullina<sup>1,2</sup>

<sup>1</sup> Mavlyutov Institute of Mechanics UFRC RAS, Ufa, Russia

<sup>2</sup> Ufa University of Science and Technology, Ufa, Russia

E-mail: buzina\_lera@mail.ru

Received April 27, 2024

Revised June 28, 2024

Accepted October 30, 2024

The dynamics of boiling a cryogenic nitrogen jet flowing through a thin conical nozzle into a vacuum chamber from a high-pressure vessel has been studied. To describe the process, a spatial axisymmetric two-phase model of a vapor–liquid mixture is proposed in a two-temperature, two-velocity, one-pressure approximations, taking into account nonequilibrium evaporation and condensation processes. The rate of mass transfer depends on number and radius of bubbles, degree of overheating in temperature, heat of vaporization, thermal conductivity coefficient and the Nusselt and Jacob numbers. The formation modes of jet flow velocity fields are studied and quantitative estimates of the spray angle magnitude in the jet are obtained depending on the initial pressure in the vacuum chamber. The reliability of the obtained results is estimated by comparison with experimental data.

**Keywords:** liquid nitrogen, boiling jet, cryogenic temperatures, vacuum chamber, numerical simulation

DOI: 10.61011/TPL.2024.12.60342.6455k

Issues related to the reliability of operation and reduction of spacecraft jet engines cost have recently become rather significant and dictate the need to conduct experimental and theoretical research aimed at studying the modes of high-speed outflow of cryogenic boiling liquids through nozzles into vacuum.

The present study provides the analysis of the influence of changes in the initial pressure in a vacuum system on the process of formation of expanding jets of liquid nitrogen sprayed from a thin cylindrical nozzle based on experimental data [1]. This work is a continuation of our previous studies [2,3], where various modes of cryogenic liquid nitrogen outflow were examined depending on the degree of superheat.

The initial temperature and pressure in a high-pressure vessel in experiments [1], which were used as the basis for analysis, were as follows:  $T_{inj} = 82.5$  K and  $p_{inj} = 4 \cdot 10^5$  Pa. Backpressure  $p_c$  in a low-pressure chamber and degree of superheat  $R_p = p_s(T_{inj})/p_c$  ( $p_s$  is the saturation pressure) for the simulated experiments are listed in Table 1. The geometric dimensions of the problem, which were set for numerical modeling in accordance with the data from [1], are given in Table 2.

A two-phase model of a vapor-liquid mixture in two-temperature, two-velocity, and one-pressure approximations with account for contact heat transfer and nonequilibrium mass-transfer processes of evaporation and condensation [4,5] was developed in order to solve this problem. The system of model equations is given in a three-dimensional Cartesian coordinate system:

mass conservation equations for phase  $i$

$$\frac{\partial(\alpha_i \rho_i)}{\partial t} + \text{div}(\alpha_i \rho_i \mathbf{v}_i) = J_{ij}, \quad (1)$$

momentum conservation equations for phase  $i$

$$\begin{aligned} \frac{\partial(\alpha_i \rho_i \mathbf{v}_i)}{\partial t} + \text{div}(\alpha_i \rho_i \mathbf{v}_i \mathbf{v}_i) \\ = -\alpha_i \nabla p + \text{div}(\alpha_i \boldsymbol{\tau}_i) + \mathbf{F}_{i,drag} + \mathbf{F}_{i,vm} + J_{ij} \mathbf{v}_i, \end{aligned} \quad (2)$$

and total energy conservation equations for phase  $i$

$$\begin{aligned} \frac{\partial(\alpha_i \rho_i E_i)}{\partial t} + \text{div}(\alpha_i \rho_i E_i \mathbf{v}_i) = -p \frac{\partial \alpha_i}{\partial t} - \text{div}(\alpha_i \mathbf{v}_i p) \\ + \text{div}(\alpha_i \gamma_{i,eff} \nabla h_i) + K_h (T_j - T_i) + \text{div}(\alpha_i \mathbf{v}_i \boldsymbol{\tau}_i) + l_s J_{ij}. \end{aligned} \quad (3)$$

The virtual mass force is

$$\mathbf{F}_{i,vm} = 0.5 \alpha_i \rho_g \left( \frac{d_i \mathbf{v}_i}{dt} - \frac{d_j \mathbf{v}_j}{dt} \right).$$

The interfacial drag is characterized by the Schiller–Naumann model:

$$\mathbf{F}_{i,drag} = \frac{3}{4} \alpha_i C_D \frac{\rho_g}{d_{i0}} (\mathbf{v}_i - \mathbf{v}_j) |\mathbf{v}_i - \mathbf{v}_j|.$$

The following notation is used in Eqs. (1)–(3):  $\rho_i$  is density,  $T_i$  is temperature,  $\alpha_i$  is volume content,  $\mathbf{v}_i$  is velocity,  $J_{ij}$  is the rate of mass transfer between phases

**Table 1.** Initial data of simulated experiments

Experiment number	Backpressure $p_c$ , $10^5$ Pa	Degree of superheat $R_p$
1	0.56	3.2
2	0.256	7.0
3	0.036	52.3

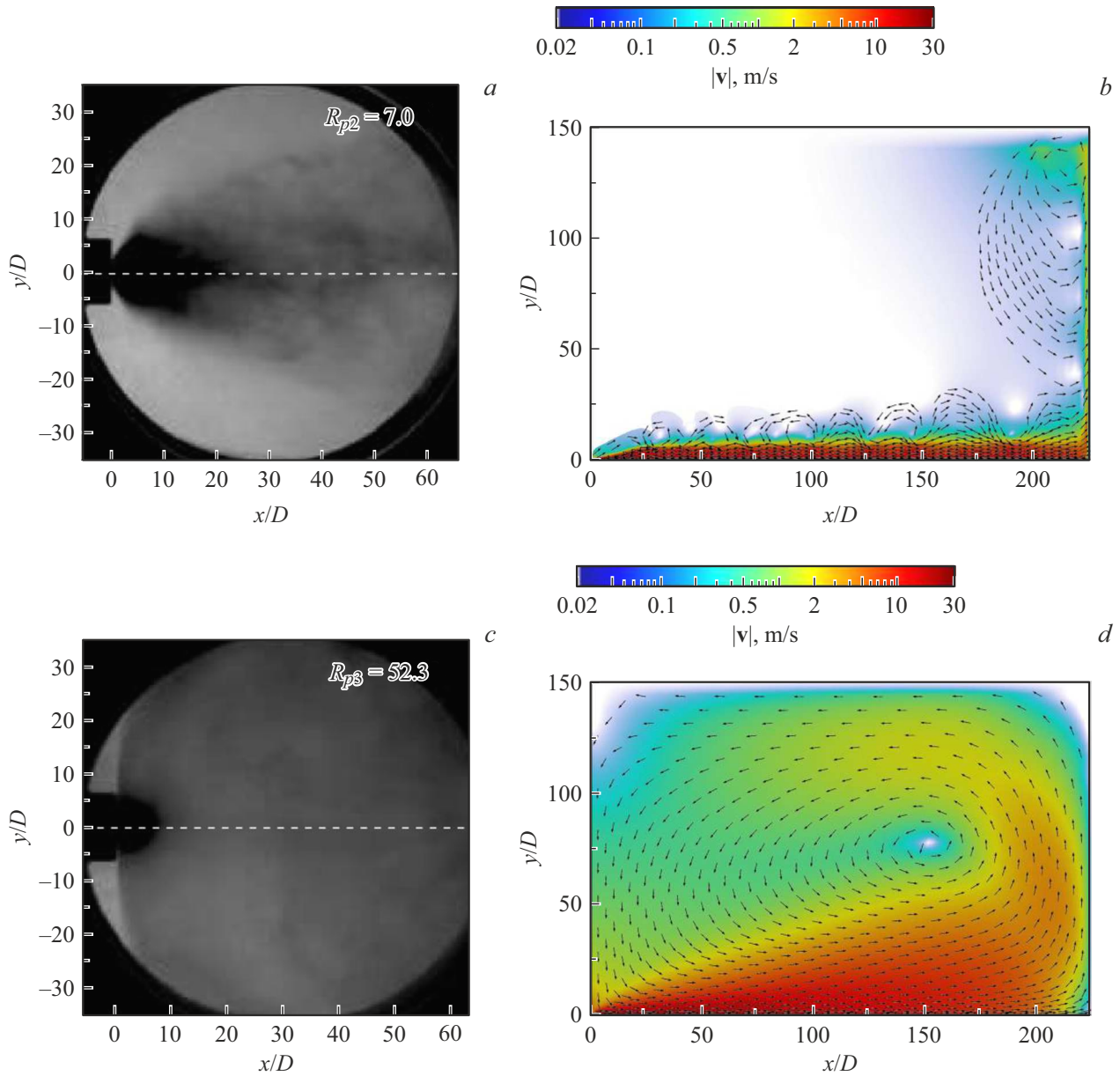


**Figure 1.** Comparison of experimental photographic images [1] (*a*, *c*) and calculated distributions of intensity and velocity vector field (*b*, *d*) for a liquid nitrogen jet at  $t = 120$  ms.  $R_{p2} = 7.0$  (*a*, *b*) and  $R_{p3} = 52.3$  (*c*, *d*).

$i$  and  $j$ ,  $p$  is pressure,  $\tau_i = \mu_i(\nabla \mathbf{v}_i + \nabla \mathbf{v}_i^T) - \frac{2}{3}(\mu_i \text{div } \mathbf{v}_i)\mathbf{I}$  is the viscous stress tensor,  $\mathbf{I}$  is a unit tensor,  $\mu_i$  is dynamic viscosity,  $E_i = e_i + K_i$  is the total energy in the form of a sum of internal and kinetic energies,  $\gamma_{i,eff}$  is effective temperature conductivity,  $h_i$  is enthalpy,  $\mathbf{v} = \alpha_l \mathbf{v}_l + \alpha_g \mathbf{v}_g$  is the velocity of a vapor-liquid mixture,  $K_{ht} = \frac{\kappa_g}{d_{l0}} \text{Nu}$  is the heat transfer coefficient,  $\kappa_g$  is the thermal conductivity of gas, Nu is the Nusselt number,  $l_s$  is the heat of vaporization/condensation, and  $d_{l0}$  is the droplet diameter. Subscripts  $i$ ,  $j$  ( $i \neq j$ ) correspond to liquid ( $l$ ) or gas ( $g$ ) phases.

The thermodynamic properties of the nitrogen gas phase are characterized by the Peng–Robinson equation of

state [6]. Following [3,7,8], we characterize the properties of liquid nitrogen by the linear in temperature and density equation of state.

In accordance with [9], evaporation rate  $J_{lg}$  is assumed to depend on number  $n$  and radius  $a$  of bubbles, saturation temperature  $T_s(p)$ , heat of vaporization  $l_s(T)$ , thermal conductivity coefficient  $\lambda_l$ , and Nusselt number Nu:

$$J_{lg} = 2\pi a n \text{Nu} \lambda_l (T - T_s(p)) / l_s(T). \quad (4)$$

The liquid–vapor phase transition occurs under nonequilibrium super-heated conditions, when the temperature of the medium exceeds the saturation temperature [3,9]:

**Table 2.** Geometric dimensions of the simulated setup

Dimension	High-pressure chamber	Intermediate pipeline	Conical nozzle	Vacuum chamber
Length $x$ , m	0.136	0.12	0.03	0.225
Radius $y$ , m	0.034	$7 \cdot 10^{-3}$	$0.5 \cdot 10^{-3}$	0.15

$T > T_s(p) + \Delta T_s$ , where  $\Delta T_s$  is the degree of superheat in temperature.

The proposed model of a vapor-liquid mixture specified by Eqs. (1)–(4) was implemented in a computational fluid dynamics package [10] with the use of a solver developed by the authors. At the internal boundaries of the computational domain, the conditions of zero normal components of phase velocities ( $v_{in} = 0$ ) are applied in accordance with the flow slip regime.

The results of numerical simulation and the corresponding experimental data [1] are presented in Figs. 1 and 2.

Figures 1, *a*, *c* show the experimental photographic images of a liquid nitrogen jet spraying at time point  $t = 120$  ms with initial injection temperature and pressure  $T_{inj} = 82.5$  K,  $p_{inj} = 4 \cdot 10^5$  Pa at degrees of superheat  $R_{p2} = 7.0$  (*a*) and  $R_{p3} = 52.3$  (*c*). Figures 1, *b*, *d* present the calculated velocity distributions in the form of a color spectrum and a field of velocity vectors (a color version of the figure is available online), which specify the flow directions obtained in the conditions similar to the experimental ones [1] (see panels *a* and *c*, respectively).

Vortex zones formed at the time point of 120 ms are visible in Figs. 1, *b*, *d*. With degree of superheat  $R_{p2} = 7.0$  (Fig. 1, *a*), multiple toroidal vortices are formed near the axis of symmetry and along the rear boundary of the vacuum chamber. At the time point under consideration, the reflection of a jet from the rear boundary and propagation to the side boundary of the chamber is revealed. The jet velocity in the axial section is  $\sim 22$  m/s. When the jet reaches the side boundary, its velocity decreases to  $\sim 5$  m/s. The jet reaches the rear surface of the vacuum chamber and the side boundary at  $t = 50$  ms and  $t = 120$  ms, respectively. In this case, the jet flow is localized along the axis of symmetry and on the rear surface (Fig. 1, *b*).

The numerical results obtained at high degree of superheat  $R_{p3} = 52.3$  (Fig. 1, *d*) revealed a fundamental change in the nature of jet flow formation (relative to the outflow mode at  $R_{p2} = 7.0$ ). The jet reaches the rear surface of the vacuum chamber and the side boundary at time points  $t = 25$  ms and  $t = 60$  ms, respectively. In this case, the flow velocity in the axial section, on reaching the side boundary, and at the front boundary is  $\sim 30$  m/s,  $\sim 10$  m/s, and  $\sim 5$  m/s, respectively.

The formation of one large toroidal vortex encompassing almost the entire vacuum chamber is seen in calculations at  $R_{p3} = 52.3$ . The direction of the velocity field of the forming vapor-droplet flow is shown in Fig. 1, *d*. It is crucial to note here that the process of formation of the maximum

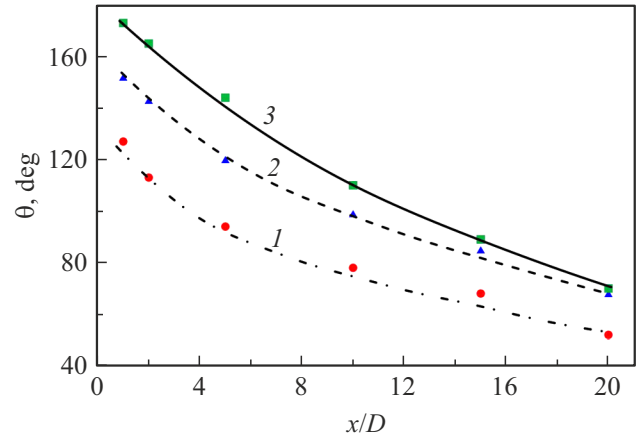


**Figure 2.** Dependence of spray angle  $\theta$  on distance  $x/D$  at degrees of superheat  $R_{p1}$  (1),  $R_{p2}$  (2), and  $R_{p3}$  (3). Symbols and curves represent the experimental data from [1] and the calculation results.

spray angle differs fundamentally from the one revealed in calculations for  $R_{p2} = 7.0$  (Fig. 1, *b*). At  $R_{p3} = 52.3$ , the spray angle is formed by the jet flow directed along the axis of symmetry, the rear and side boundaries, the front boundary, and the main jet flowing out of the nozzle. At the time point of 120 ms, the maximum jet spray angle is formed by the reverse jet flow, which is illustrated by the velocity vector field in Fig. 1, *d*.

Figure 2 presents a comparison of experimental points and calculated dependences of the spray angle in sections located at distances  $x/D$  from the nozzle. The degrees of superheat are  $R_{p1} = 3.2$ ,  $R_{p2} = 7.0$ , and  $R_{p3} = 52.3$ . Spray angles  $\theta$  for experiments [1] were obtained using the algorithm of post-processing of shadow images of the formed jet at time  $t = 120$  ms.

Thus, the study of dependences of the spray angle of a liquid nitrogen jet on the degree of superheat performed by implementing model (1)–(4) numerically revealed that the largest spray angle is found in the near field of the nozzle ( $x/D = 1$ ). The jet expansion angle increases with degree of superheat. The spray angle decreases with distance from the nozzle, which is consistent with the experimental data from [1].

Calculations revealed certain features of formation of velocity directions of the vapor-droplet flow at degree of superheat  $R_{p3} = 52.3$  that are induced by the emergence of reverse flows forming jet spray angle  $\theta_{R_{p3}}^{calc} \approx 180^\circ$ , which was observed experimentally [1] (Figs. 1, *c* and 2).

## Funding

This study was supported by the Russian Science Foundation, grant № 23-29-00309 (<https://rscf.ru/en/project/23-29-00309/>).

## Conflict of interest

The authors declare that they have no conflict of interest.

## References

- [1] A. Rees, H. Salzmann, J. Sender, M. Oswald, in *8th Eur. Conf. for aeronautics and space sciences (EUCASS)* (Madrid, Spain, 2019). DOI: 10.13009/EUCASS2019-418
- [2] R.Kh. Bolotnova, V.A. Korobchinskaya, E.F. Gainullina, *Lobachevskii J. Math.*, **44** (5), 1579 (2023). DOI: 10.1134/S1995080223050104
- [3] R.Kh. Bolotnova, V.A. Korobchinskaya, E.F. Gainullina, *Tech. Phys. Lett.*, **49** (12), 108 (2023). DOI: 10.61011/TPL.2023.12.57601.107A.
- [4] R.I. Nigmatulin, *Dynamics of multiphase media* (Hemisphere, N.Y., 1990).
- [5] L.D. Landau, E.M. Lifshitz, *Course of theoretical physics. Fluid mechanics* (Pergamon, N.Y., 1987).
- [6] D.Y. Peng, D.B. Robinson, *Ind. Eng. Chem. Fundamen.*, **15** (1), 59 (1976). DOI: 10.1021/i160057a011
- [7] R.I. Nigmatulin, R.Kh. Bolotnova, *High Temp.*, **49** (2), 303 (2011). DOI: 10.1134/S0018151X11020106.
- [8] V.V. Sychev, A.A. Vasserman, A.D. Kozlov, G.A. Spiridonov, V.A. Tsymarnyi, *Termodinamicheskie svoistva azota* (Izd. Standartov, M., 1977) (in Russian).
- [9] R.Kh. Bolotnova, V.A. Buzina, M.N. Galimzyanov, V.Sh. Shagapov, *Teplofiz. Aeromekh.*, **19** (6), 719 (2012) (in Russian).
- [10] *OpenFOAM. The open source computational fluid dynamics (CFD) toolbox* [Electronic source]. <http://www.openfoam.com>

*Translated by D.Safin*